Tropical Rainfall and Boundary Layer Moist Entropy

IAN FOLKINS AND CHRISTOPHER BRAUN

Department of Physics and Atmospheric Science, Dalhousie University, Halifax, Nova Scotia, Canada

ABSTRACT

In the Tropics, the variation of rainfall with sea surface temperature (SST) is highly nonlinear. Rainfall shows no dependence on SST for SST increases from 19° to 26°C, abruptly increases by a factor of 5 as SSTs increase from 26° to 29°C, and then rapidly declines. It is argued that this nonlinear dependence is a response to the nonlinear dependence of convective mass on SST. Convective mass is a measure of the mass in the convective boundary layer thermodynamically able to participate in deep convection by virtue of its positive convective available potential energy (CAPE). Monthly mean estimates of convective mass were obtained at various islands in the tropical Pacific and Caribbean from the NOAA/National Climatic Data Center high-resolution radiosonde database. In the inner Tropics, the tendency for temperatures above the boundary layer to be homogeneous plays an important role in the rapid increase in rainfall near the convective threshold SST. At SSTs below the convective threshold, near-surface winds are generally directed from cold to warmer SSTs, so that horizontal advection of equivalent potential temperature (θ_e) will tend to suppress moist entropy, and rainfall, in these regions. In areas of the ocean with SSTs larger than the convective threshold, the mean frequency distribution of θ_e in the boundary layer becomes independent of SST. This occurs both as a response to the homogeneity of temperatures in the inner Tropics, and to the tendency for wind speeds in the boundary layer to decrease with SST for SSTs larger than the convective threshold. In the subtropics, temperature fluctuations are much larger than in the inner Tropics, and can be expected to play a much greater role in determining precipitation patterns.

1. Introduction

In the Tropics, thunderstorms and rainfall tend to occur more frequently over regions with higher sea surface temperatures (SSTs). It was originally suggested that this relationship was due to the existence of higher heat and moisture fluxes from the ocean at high SSTs (Ichiye and Petersen 1963; Bjerknes 1966). But there soon emerged several very puzzling aspects of the rainfall–SST relationship, which brought into question the idea that this relationship could be understood purely in terms of local air–sea fluxes. During the latter stages of the 1972–73 ENSO event, rainfall at Kanton (an island at 2.5°S in the Central Pacific) decreased dramatically as the warm pool retreated and SSTs went below 28°C (Ramage 1977). However, this decrease in rainfall was associated with an increase in the sum of sensible and latent heat fluxes from the ocean. On the island of Baltra (near the Galapagos), where SSTs remained somewhat colder, there was no correlation between SST and rainfall. Many other studies have since shown (Gill and Rasmusson 1983; Gadgil et al. 1984; Graham and Bar-

nett 1987; Waliser et al. 1993; Zhang 1993) that although rainfall and the frequency of high cloud show little sensitivity to changes in SST for SSTs below 26°C, rainfall rapidly increases in going from an SST of 26° to 28°C. Somewhat surprisingly, rainfall and the frequency of high cloud then appear to diminish as SSTs go above 29.5°C. In contrast, the latent heat flux tends to increase very slowly with SST until 28°C, then declining at the highest SSTs, due both to an increase of relative humidity in the boundary layer, and a decrease in wind speed (Zhang and McPhaden 1995; Zhang et al. 1995).

There is now a widely accepted theoretical expectation that tropical deep convection should be controlled by the distribution of subcloud layer entropy, and that SST is but one of the factors that can influence this distribution (Neelin and Held 1987; Emanuel et al. 1994; Raymond 1994, 1995, 2000). There have, however, been few observational studies of the distribution of subcloud-layer entropy and its climatological relationships with SST and rainfall. In this paper, we use temperature and humidity profiles from the National Oceanic and Atmospheric Administration National Climatic Data Center (NOAA/NCDC) high-resolution radiosonde database to examine the relationships between subcloud-layer entropy (θ_e), rainfall, and SST in the Tropics.

Corresponding author address: Dr. Ian Folkins, Department of Physics and Atmospheric Science, Dalhousie University, Halifax, NS B3H 3J5, Canada.
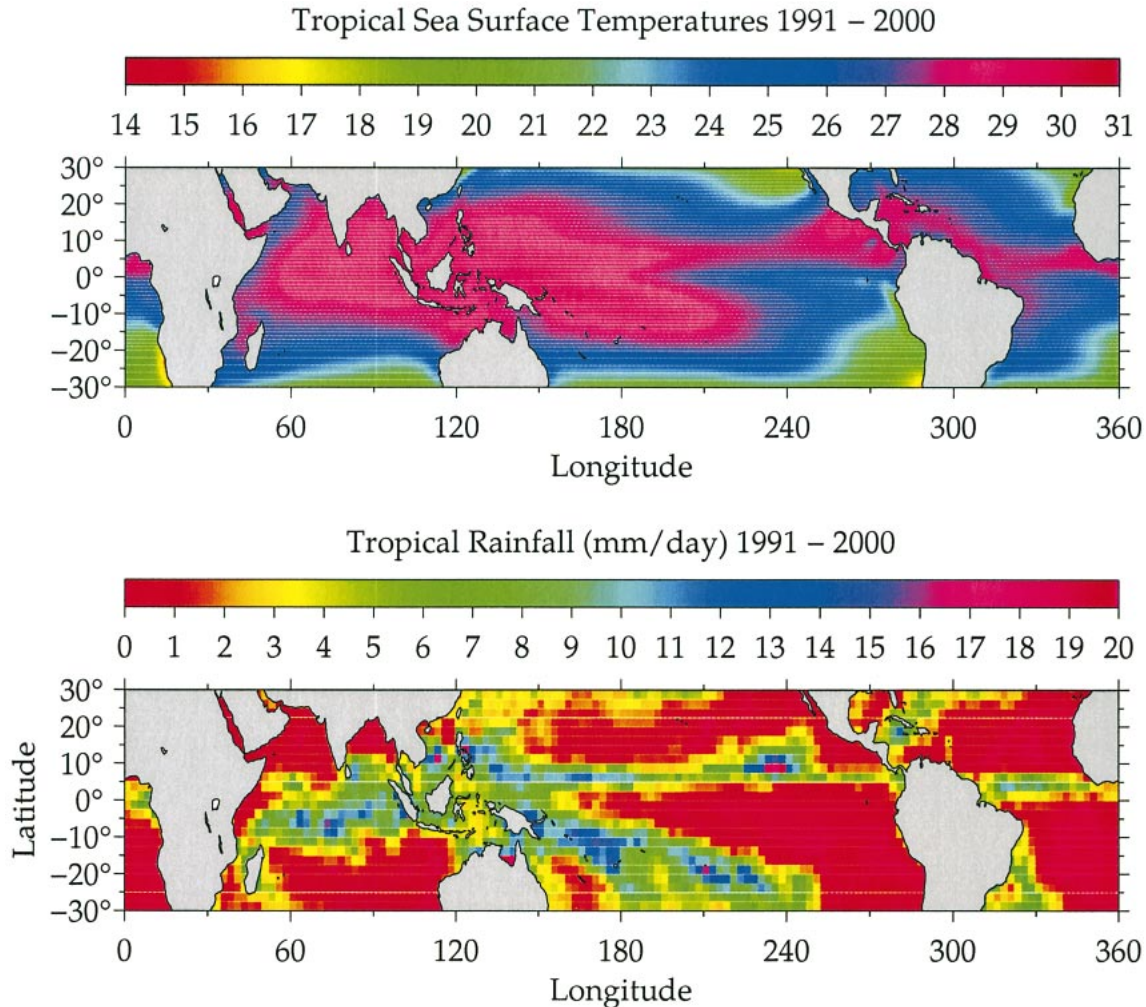E-mail: Ian.Folkins@dal.ca

FIG. 1. (top) The climatological distribution of SST in the Tropics from 1991 to 2000 (Reynolds et al. 2002). (bottom) The climatological distribution of precipitation over the oceans from 1991 to 2000 from the GPCP Version 2 Combined Precipitation Data Set (Huffman et al. 1997).

The concepts of convective threshold pseudoequivalent potential temperature ($\theta_{e,\mathrm{conv}}$) (Raymond 1995) and convective mass play a central role in our analysis. The $\theta_{e,\mathrm{conv}}$ of a temperature profile is defined as the θ_e at which the convective available potential energy (CAPE) of an air parcel in the boundary layer first becomes positive. When an air parcel at the surface has $\theta_e > \theta_{e,\mathrm{conv}}$, it will be positive buoyant in the midtroposphere when lifted upward along a moist pseudoadiabatic trajectory. Temperatures in the inner Tropics tend to approximate a moist pseudoadiabat below 11 km, so that the moist pseudoadiabat of the convective threshold θ_e tends to approximate the observed temperature profile in much of the tropical troposphere. The convective mass is defined as the mass of air in the boundary layer (below 800 mb) whose θ_e exceeds $\theta_{e,\mathrm{conv}}$. It is a measure of the mass of air in the boundary which, by virtue of its positive CAPE, is thermodynamically able to participate in deep convection. We find that the climatological

dependence of convective mass on SST is similar to the climatological dependence of rainfall on SST. This suggests that the nonlinear dependence of tropical rainfall on SST might be better understood by an examination of the reasons for the nonlinear dependence of boundary layer convective mass (moist entropy) on SST in the Tropics.

2. Tropical rainfall and sea surface temperatures

The top panel of Fig. 1 shows the climatological distribution of sea surface surface temperatures in the Tropics. It was obtained by averaging over $1° \times 1°$ monthly mean SSTs (Reynolds et al. 2002) from 1991 to 2000. The lower panel shows the climatological distribution of rainfall over the tropical oceans. It was obtained by averaging over the $2.5° \times 2.5°$ monthly mean rainfall estimates from the Global Precipitation Climatology Project (GPCP) Version 2 Combined Precipitation Data

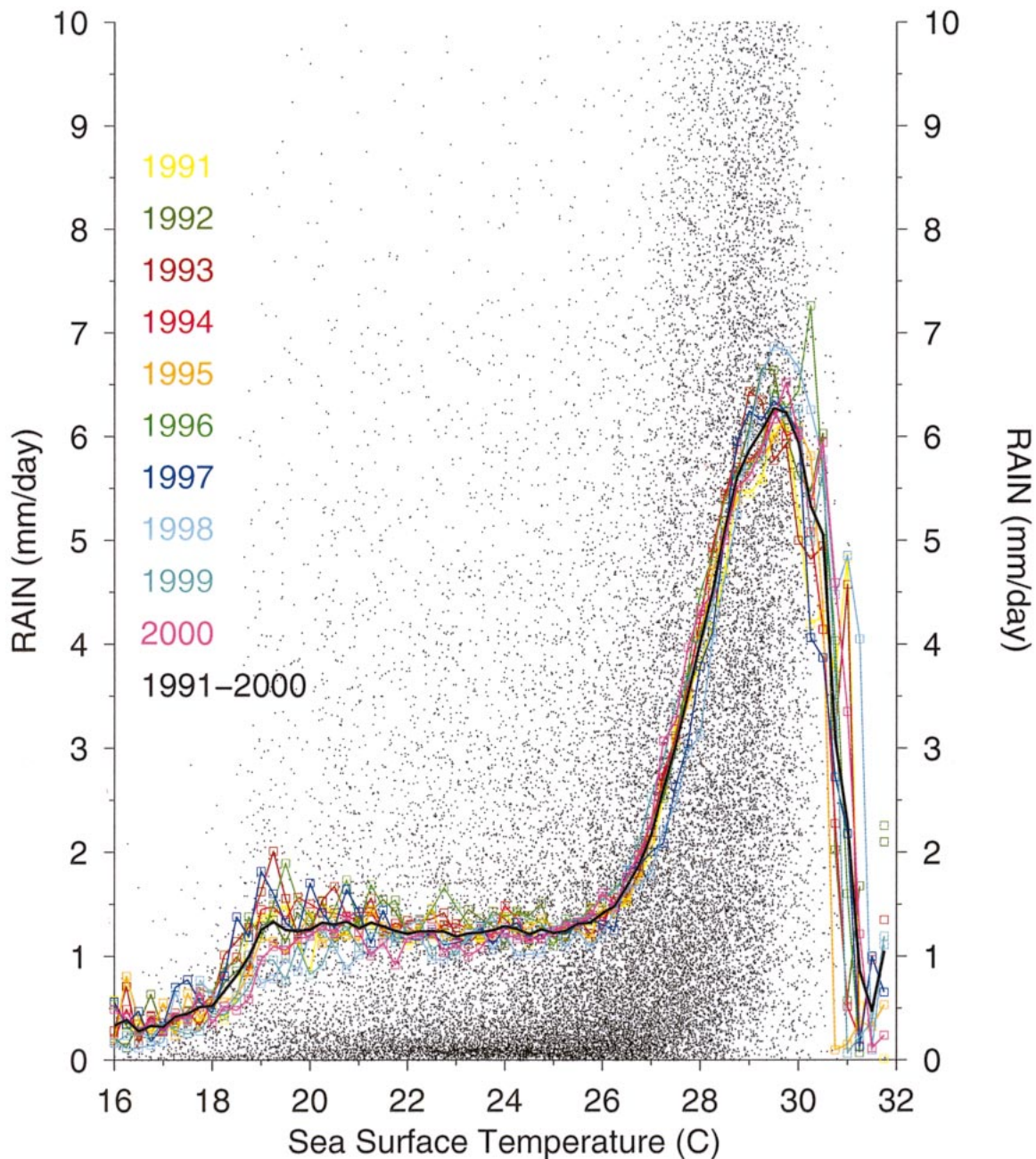FIG. 2. A scatterplot of 2.5° × 2.5° monthly mean GPCP rainfall over the tropical oceans (30°S–30°N) plotted against the corresponding monthly mean SST value (originally in 1° resolution but averaged over the GPCP rainfall pixels). The scatterplot shows data from 1991 only (other years are similar). The colored lines represent averages from particular years using all data from that year. The solid black line is the 1991–2000 average.

Set (Huffman et al. 1997), also from 1991 to 2000. A visual comparison of the two panels suggests the existence of a threshold SST of about 28°C at which mean rainfall goes above 3 mm day^{-1}.

In Fig. 2, each monthly mean GPCP rainfall estimate between 30°S and 30°N from 1991 is plotted against the corresponding monthly mean Reynolds SST, averaged over the 2.5° × 2.5° rainfall bin. The large amount of

scatter in the relationship indicates some of the difficulties encountered in attempting to predict tropical rainfall from SST alone (Weare 1987). There is, however, a mean dependence of tropical rainfall on SST that is quite reproducible from year to year. Each of the lighter curves in Fig. 2 is the mean rainfall–SST relationship for one of the years from 1991 to 2000; the thicker black curve is the 1991–2000 average. It con-
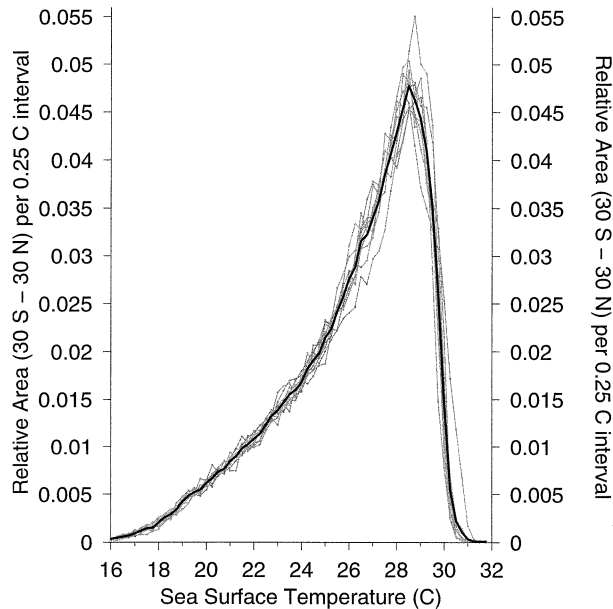
FIG. 3. The frequency distribution of SSTs in the Tropics (30°S–30°N). The gray lines represent averages from individual years, while the solid black line is the 1991–2000 average.

firms some of the elements of the mean rainfall–SST relationship discussed earlier: the weak dependence of rainfall on SST for SSTs below 26°C, the onset of a rapid increase in rainfall at 26°C, a rainfall maximum at 29.5°C, and a decrease of rainfall at the highest SSTs. It is also interesting, that in the El Niño years of 1997 and 1998, the threshold SST is shifted to a slightly larger value. Some the very high SST but low rainfall points in Fig. 2 originate from the Red Sea, where deep convection would be inhibited by the surrounding very dry boundary layer.

Figure 3 shows a probability distribution function (PDF) of SSTs in the Tropics (30°S–30°N). The PDF was obtained by adding up the total area in each 0.25°C SST bin from the Reynolds analysis with, again, the lighter plots representing an individual year from 1991 to 2000, and the thick black line representing the average from the entire period. The most intriguing aspects of this distribution are probably the slow buildup in SST area until a maximum at 28°C, and the subsequent very rapid decrease. In particular, areas with SSTs larger than 30°C are extremely rare. Those with SSTs larger than 31°C are virtually nonexistent. Under clear-sky conditions, the surface heat budget of the tropical ocean balances near 30°–31°C (Newell 1979). A 30% reduction in solar radiation due to clouds, as might be expected in regions of active deep convection, reduces the local steady-state SST to 28°C (Graham and Barnett 1987; Ramanathan and Collins 1991), and probably helps account for the peak in the PDF at this temperature. Figure 2 shows that areas with SSTs in excess of 30°C are associated with reduced rainfall, as well as reduced high cloud (Graham and Barnett 1987). The rarity of ocean

"hot spots" is therefore probably attributable to the rarity of the dynamical conditions capable of inhibiting deep convection over extremely warm regions of the ocean (e.g., Waliser 1996).

3. Convective mass

The CAPE of an air parcel at the surface is defined as

$$\text{CAPE} = \int_{\text{Surf}}^{\text{LNB}} (T_{\text{vp}} - T_{\text{vb}})R_d \, d \ln P, \qquad (1)$$

where T_{vb} is the virtual temperature of the background atmosphere, T_{vp} is the virtual temperature of an air parcel lifted upward from the surface along a moist pseudoadiabat with some initial surface temperature, pressure, and relative humidity, R_d is the ideal gas constant, P the pressure, and the integral goes from the surface to the level of neutral buoyancy. Although the presence of water vapor increases both T_{vp} and T_{vb}, the effect on T_{vp} is usually larger since the rising air parcel will tend to be at or near saturation.

Given a background virtual temperature profile, there are various combinations of initial temperature, relative humidity, and pressure, which will generate pseudoadiabatic profiles with zero CAPE. This means that $\theta_{e,\text{conv}}$ is not uniquely determined. In our calculations, the initial starting pressure of the air parcel was set equal to the surface pressure, and the initial surface relative humidity was fixed at 0.75. We then determined a $\theta_{e,\text{conv}}$ by first starting out with an initial surface temperature, which would generate a large positive CAPE, and then progressively decreasing the temperature until we found one for which CAPE = 0. We then used this combination of initial pressure, relative humidity, and temperature to calculate $\theta_{e,\text{conv}}$ (Bolton 1980). It can be shown that increasing the initial relative humidity of the air parcel increases the $\theta_{e,\text{conv}}$ generated by this procedure. For example, starting out with a perhaps slightly more realistic initial relative humidity of 0.85 would have increased $\theta_{e,\text{conv}}$ by about 0.15 K. The initial surface temperature is, of course, in this case reduced. Starting out with a pressure slightly lower than surface pressure tends to decrease $\theta_{e,\text{conv}}$. For example, $\theta_{e,\text{conv}}$ decreases by about 0.45 K in going from 1000 to 950 mb. Although it is important to keep these differences in mind, they do not significantly affect our subsequent calculations of convective mass, and as will be seen, are smaller than current uncertainties in the measurement of θ_e. They are also smaller than the more basic uncertainty of whether one should lift the air parcel along a reversible moist adiabat (Xu and Emanuel 1989) or an irreversible pseudoadiabat. During pseudoadiabatic ascent, condensate is removed from the air parcel as soon as it is formed. This ignores possible changes in the buoyancy and specific heat of rising air parcels due to the retention of water and/or ice.

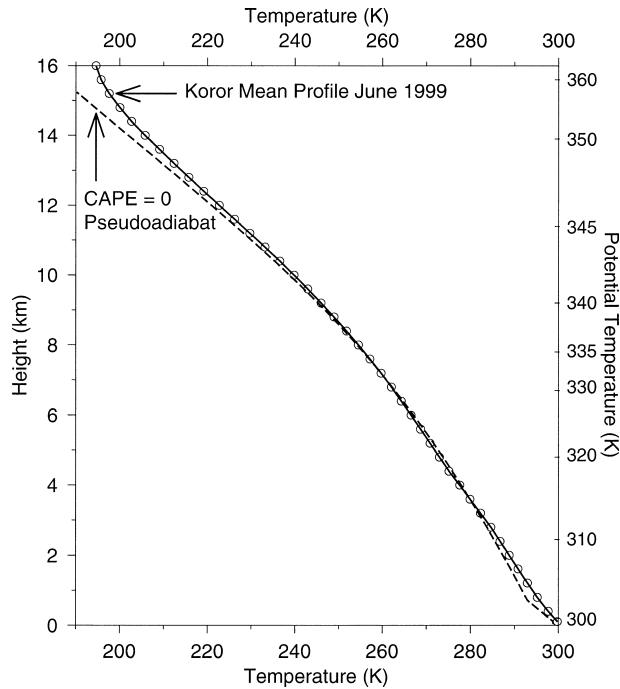In Fig. 4, the curve with open circles is the mean

FIG. 4. The solid line with open circles is the mean temperature profile above Koror for Jun 1999. The dashed line is the moist pseudoadiabat of the monthly mean $\theta_{e,\mathrm{conv}}$ (in this case 343.8 K).
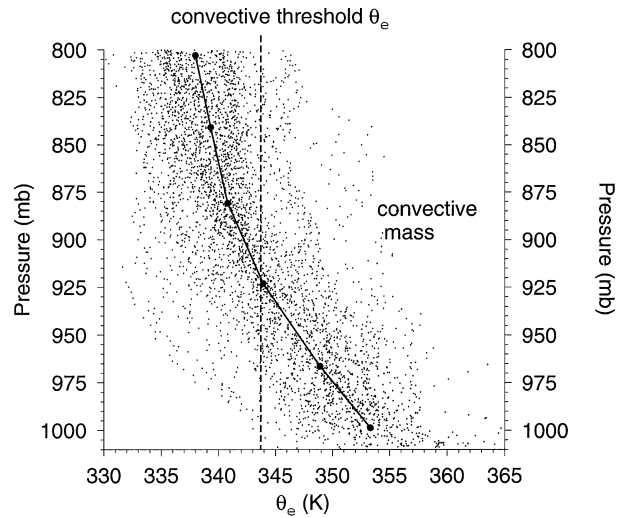

FIG. 5. A scatterplot of θ_e against pressure from all 60 radiosonde profiles above Koror in Jun 1999. The solid line is the mean θ_e profile. Air parcels whose θ_e exceeds $\theta_{e,\mathrm{conv}}$, i.e., those to the right of the vertical dashed line, contribute to the local convective mass.

temperature profile over Koror (7.3°N, 134.5°E) for the month of June 1999. It is an average over the 60 NOAA/NCDC high-resolution radiosonde temperature profiles available for this month. This radiosonde data was downloaded from the Stratospheric Processes and their Role in Climate (SPARC) Data Center (available online at www.sparc.sunysb.edu). We generated a $\theta_{e,\mathrm{conv}}$ for each of the 60 virtual temperature profiles above Koror in June, 1999 using the procedure discussed above. The moist pseudoadiabat of the monthly mean $\theta_{e,\mathrm{conv}}$ is represented in Fig. 4 by the dashed line. This pseudoadiabat has near-zero CAPE because the small negative contribution to CAPE near the surface (convective inhibition) is cancelled by the positive contributions to CAPE from higher levels. (The use of temperature rather than virtual temperature in Fig. 4 exaggerates the magnitude of the convective inhibition.) While the observed temperature profile follows the $\theta_{e,\mathrm{conv}}$ moist pseudoadiabat in much of the troposphere, it increasingly deviates from the moist pseudoadiabat above 11 km.

Figure 5 shows a scatterplot of θ_e against pressure, calculated from simultaneous measurements of pressure, temperature, and relative humidity above Koror in June 1999. The solid line is the mean θ_e profile above Koror for this month. Air parcels whose θ_e exceeds the monthly mean $\theta_{e,\mathrm{conv}}$ occur throughout the convective boundary layer (CBL), but are observed more frequently closer to the surface. The monthly mean convective mass was calculated by finding the mean fraction of air parcels in each 10-mb layer from 1010 to 800 mb whose

θ_e exceeded the $\theta_{e,\mathrm{conv}}$ for that radiosonde profile, multiplying this by 10 mb, and adding up the contributions from each 10-mb layer.

Figure 6 shows the monthly mean convective mass plotted against the corresponding monthly mean Reynolds SST for each of the radiosonde stations in the
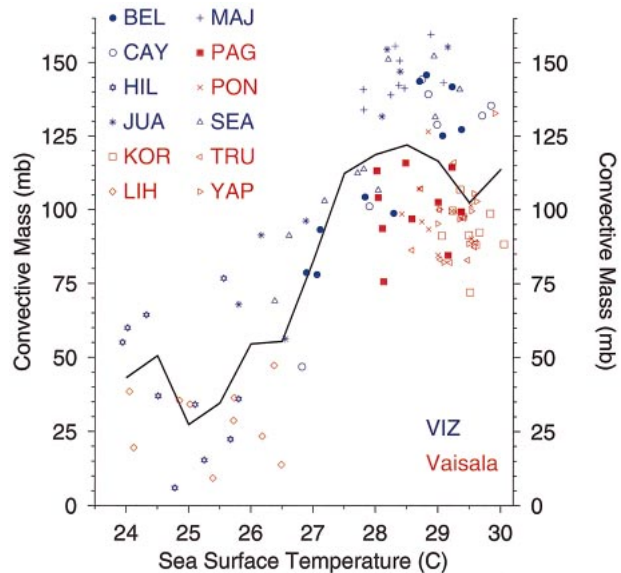

FIG. 6. A plot of the monthly mean convective mass against the local monthly mean SST at each of the radiosonde locations. The solid line represents the mean dependence of convective mass on SST, averaged in 0.5°C intervals. The convective mass is the amount of mass in the convective boundary layer (below 800 mb) whose θ_e exceeds $\theta_{e,\mathrm{conv}}$. The locations corresponding to the three letter codes are shown in Fig. 7. Convective masses calculated using relative humidity measurements using Vaisala sondes are shown in red, while those using VIZ sondes are shown in blue.
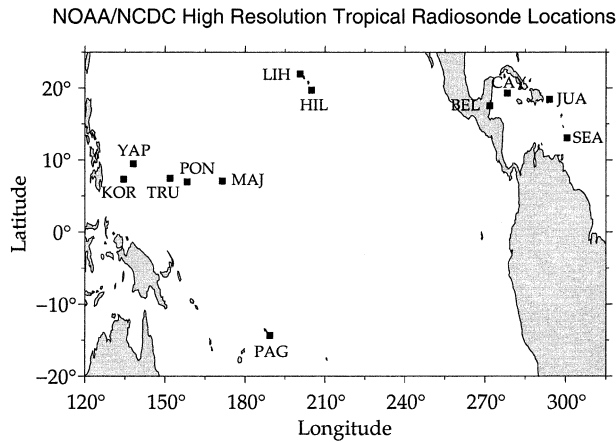
FIG. 7. Locations of the tropical NOAA–NCDC radiosondes used in this paper. Each location has been identified by a three letter code, BEL: Belize, CAY: Grand Cayman, HIL: Hilo (Hawaii), JUA: San Juan/Isla Verde (U.S.), KOR: Koror/Palau Island, LIH: Lihue/Kauai (Hawaii), MAJ: Majuro/Marshall Island, PAG: Pago Pago International Airport (Samoa), PON: Ponape Island, SEA: Seawell (Barbados), TRU: Truk Intl/Moen Island, YAP: Yap Island.
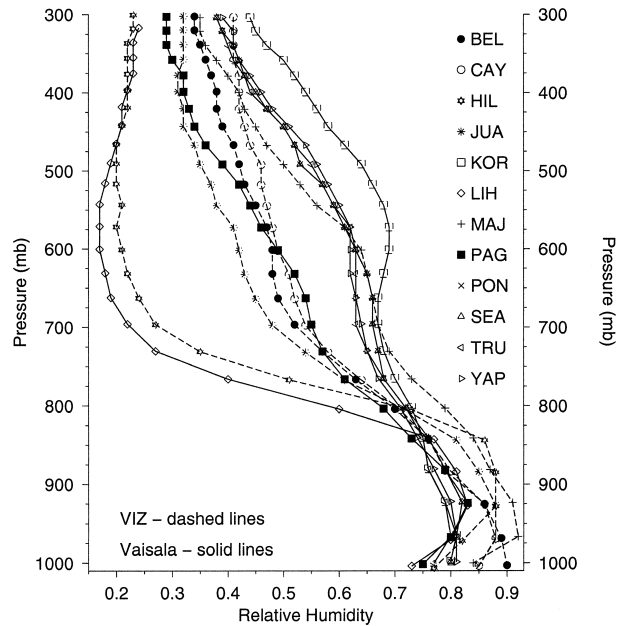

FIG. 8. Annual mean relative humidity climatologies from the 12 radiosonde locations. Measurements from Vaisala sondes are shown using solid lines, while those from VIZ sondes are shown using dashed lines. Below 800 mb, relative humidities from the VIZ sondes are consistently higher than humidities from the Vaisala sondes.

NOAA/NCDC high-resolution database. Where possible, all 12 months from 1999 for each of the stations were used. The locations of these stations are shown in Fig. 7. The solid line in Fig. 6 represents the average dependence of convective mass on SST, obtained by averaging over all sites in 0.5°C bins. For SSTs of between 24° and 26°C, the convective mass is about 40 mb. Between 26° and 28°C, the average convective mass increases by about a factor of three in going from 40 to 120 mb. The proximity of this increase to the convective threshold SST supports the notion that the existence of the threshold is related to changes in the amount of low-level θ_e exceeding $\theta_{e,\mathrm{conv}}$ (Betts and Ridgway 1989).

Figure 6 also shows that the convective mass calculated from stations using VIZ sondes (shown in blue) is consistently higher than that calculated from stations using Vaisala sondes (shown in red). This bias appears to originate mainly from differences in the way the two types of sondes measure relative humidity in the boundary layer. Figure 8 shows the annual mean relative humidity profiles at each of the 12 sites, using all data from 1999. All stations have high relative humidities in the CBL (below 800 mb). However, relative humidities in the CBL from stations using the VIZ sondes (dashed lines) are consistently higher than those using the Vaisala sondes. For example, the annual mean relative humidity below 800 mb at station HIL is consistently 3%–10% higher than the humidity at the nearby station LIH, and the relative humidity at the VIZ station MAJ is consistently 10% higher than the four nearby stations in the western tropical Pacific using Vaisala sondes. Relative humidity measurements using Vaisala sondes from the 1992 to 1993 the Tropical Ocean Global Atmosphere Coupled Ocean–Atmosphere Response Experiment

(TOGA COARE) campaign exhibited a dry bias that has been well characterized (Wang et al. 2002). Changes to the Vaisala sondes introduced in September 1998 are expected to have reduced the dry bias by 30%–50%. A second change, introduced since the data used in this paper were taken, is expected to have eliminated the dry bias. Relative humidities from the VIZ sondes are expected to have a moist bias of <4% at relative humidities exceeding 70% (J. Wang 2002, personal communication).

Figure 9 shows the annual mean pseudoequivalent potential temperature (θ_e) profiles at each of the 12 locations. The profiles tend to fall in three groups, depending on whether the site is in Hawaii, the Caribbean or Samoa, or the western tropical Pacific. At the site MAJ, the moist bias of the VIZ sonde gives rise to an annual mean θ_e that is higher than its four neighboring sites. This difference is near zero at 800 mb, but is 5 K through much of the CBL.

4. Convective water

During a convective event, one might expect most of the convective mass to be removed from the CBL. The total amount of moisture in an updraft would then be equal to the total amount of water vapor initially present in the convective mass. We refer to this as the convective water. To determine the convective water, we first calculated the mean dependence of the water vapor mass mixing ratio on θ_e in every 1°C SST bin from 24° to 30°C, using all data below 800 mb. Within each SST
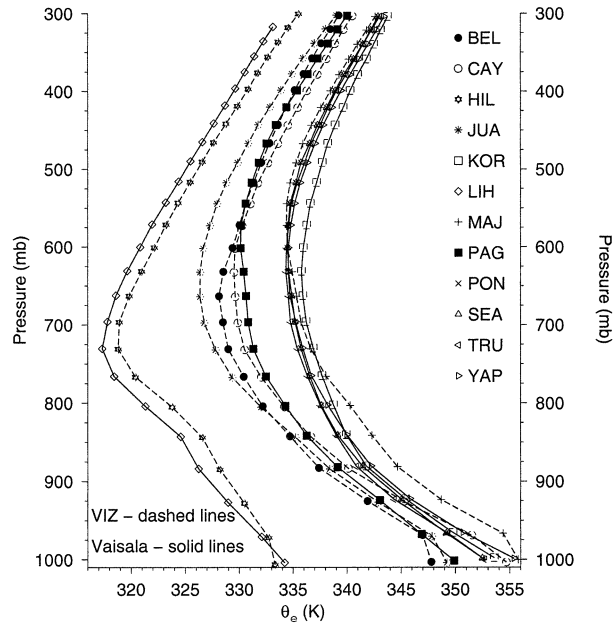
FIG. 9. Annual mean θ_e climatologies from the 12 radiosonde stations. Profiles obtained using Vaisala sondes are shown using solid lines, while those obtained from VIZ sondes are shown using dashed lines. In general, the profiles tend to subdivide into three groups, with the two profiles with the lowest θ_e from Hawaii, the group of four intermediate profiles from the Caribbean, and the six profiles with the largest θ_e from the western tropical Pacific.
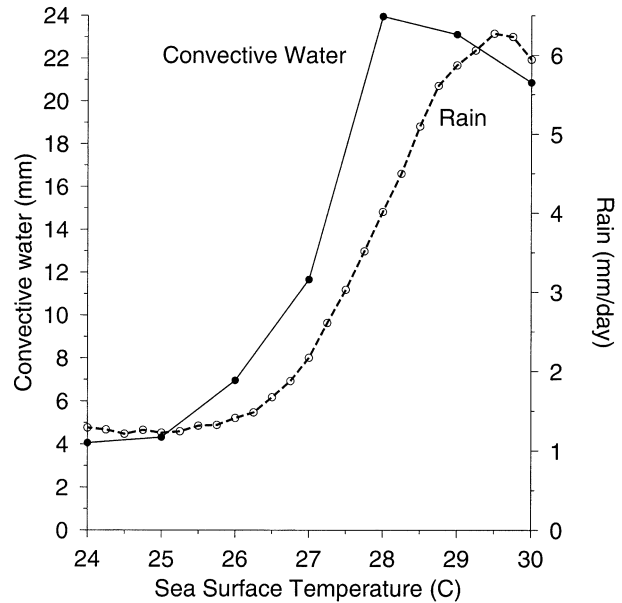

FIG. 10. The solid line shows the dependence of mean convective water on SST calculated from the 12 radiosonde locations. The convective water represents the amount of water that would be obtained by extracting all the water vapor from air parcels in the boundary layer whose θ_e exceeds $\theta_{e,conv}$. The dashed curve shows the dependence of the mean 1990–2000 tropical rainfall on SST (also shown in Fig. 2).

bin, we also calculated the mean dependence of convective mass on θ_e. The total convective water at each SST was then set equal to the product of $r_{SST}(\theta_e)$ and the convective mass at that θ_e, integrated over all $\theta_e > \theta_{e,conv}$. The mean dependence of convective water on SST, generated by this method, using all 1999 data from the 12 radiosonde stations shown in Fig. 7, is shown in Fig. 10. Also shown in Fig. 10 is the climatological dependence of rainfall on SST in the Tropics, shown previously in Fig. 2. The similarity in the shape of the two curves suggests that, on long timescales, the rainfall rate in the Tropics is at least partially controlled by the amount of water vapor in the boundary layer thermodynamically able to participate in deep convection.

One might think that the mean residence time of a water molecule in the CBL, once the θ_e of the air parcel exceeds the local $\theta_{e,conv}$, would equal the convective water divided by the rain rate. This would give rise to a convective removal timescale τ_{rem} of about 3.7 days. However this estimate ignores the fact that much of the rainfall in the Tropics evaporates as it falls to the ground, and that many of the smaller convective plumes will mix with dryer air in the mid- and lower troposphere, generating little if any precipitation. It has been suggested that the tropical mean precipitation efficiency, i.e., the fraction of condensate that reaches the surface, is about 60% (Emanuel 1994). If so, a rain rate of 6 mm day^{-1}, as is characteristic of regions where the local SST exceeds 28°C, would imply a net rate of removal

of water from the CBL of about 10 mm day^{-1}, or perhaps somewhat more, after taking into account nonprecipitating convection, which also exports water vapor from the boundary layer. Since the amount of convective water in the CBL at these temperatures is about 22 mm, the timescale at which convective mass is removed from the CBL is about 2 days. This 2 day estimate for τ_{rem} is consistent with a previous estimate generated by calculating the mean deep convective detrainment rate between adjacent potential temperature surfaces in the upper tropical troposphere (Folkins 2002). The detrainment rate was then compared with the amount of mass in the boundary layer between the two corresponding θ_e values that would be required to sustain this detrainment rate. The resulting 2-day estimate for τ_{rem} appeared to be roughly independent of θ_e.

5. Variations in $\theta_{e,conv}$

Although one tends to attribute the existence of tropical convection to the presence of warm moist air near the surface, convection arises from a competition between the moist entropy of the CBL and the temperature of the atmosphere. Although temperatures in the inner Tropics (10°S–10°N) tend to be quite homogeneous, temperature fluctuations in the subtropics, often associated with midlatitude systems, can be substantial, and play an important role in modulating the frequency of subtropical deep convection (Kiladis and Weickmann 1992; Slingo 1998). Figure 11 shows the local monthly
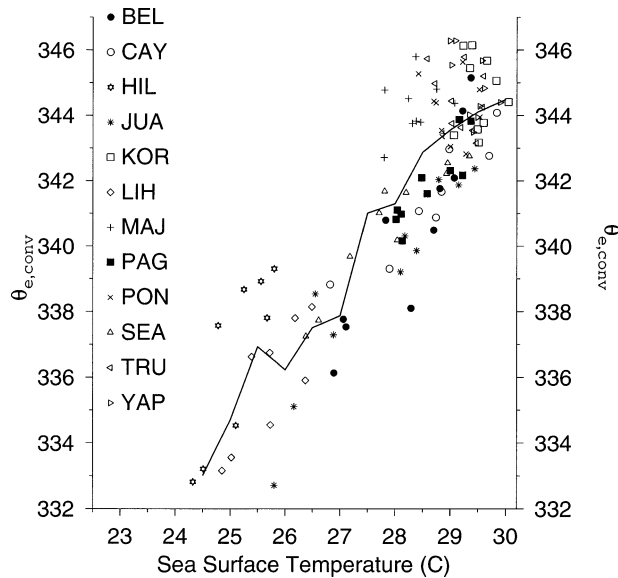
FIG. 11. A scatterplot of the monthly mean $\theta_{e,conv}$ against monthly mean SST at the 12 radiosonde locations. The locations corresponding to the three letter codes are shown in Fig. 7. The solid curve is the mean dependence of $\theta_{e,conv}$ on SST, averaged in 0.5°C intervals.

FIG. 12. Annual mean probability distribution functions of $\theta_{e,conv}$ at the six western tropical Pacific stations (open circles), the three Caribbean and one Samoan station (solid circles), and the two Hawaiian stations (open squares).

mean $\theta_{e,conv}$ plotted against the local SST for all 12 radiosonde locations. For the radiosonde locations used in this study, $\theta_{e,conv}$ rapidly increases from 334 to 342 K in going from an SST of 25° to 28°C. It then tends to stabilize for SSTs larger than 28°C.

It should be kept in mind, however, that all of the sites with SSTs below 27.5°C used in this analysis are located in Hawaii or the Caribbean, while most of the sites with SSTs higher than 27.5°C are located in the western Pacific warm pool. The dependence of $\theta_{e,conv}$ on SSTs shown in Fig. 11 may therefore not be representative of the Tropics as a whole. In particular, the inclusion in Fig. 11 of radiosonde stations closer to the equator, but with SSTs below 27.5°C, would tend to increase $\theta_{e,conv}$ at low SST, and thereby lower the mean convective mass at low SSTs.

Figure 12 shows probability distribution functions of $\theta_{e,conv}$ from the three regions used in this study, obtained from individual radiosonde profiles. Over the western Pacific warm pool sites, the most likely $\theta_{e,conv}$ is 344 K, with almost all values falling between 341 and 348 K. In going from the inner Tropics to the Caribbean locations, and then to Hawaii, the most likely $\theta_{e,conv}$ is progressively reduced, and the variance increases. Some of this increased variance is probably associated with the increased amplitude of the seasonal temperature cycle at these locations. In any event, the increased variance in $\theta_{e,conv}$ over the cooler SST subtropical locations can be expected to be associated with increased fluctuations of convective mass, and help give rise, as shown in Fig. 2, to the occasionally very large rainfall rates observed at these locations.

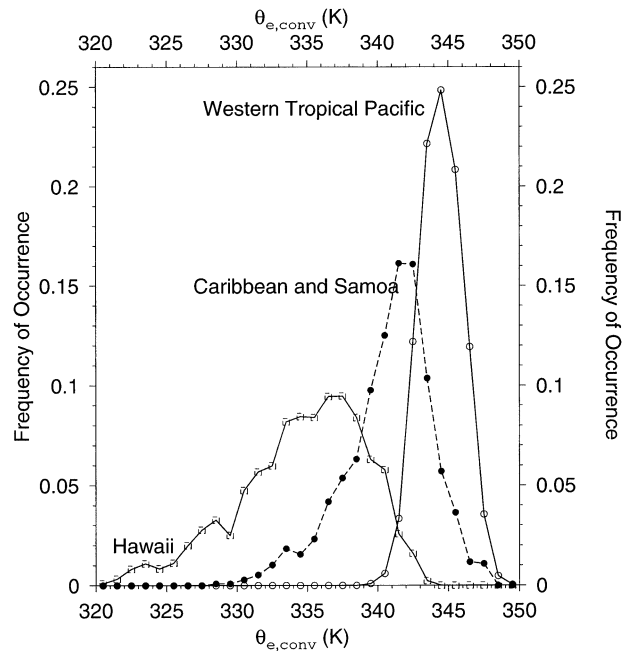One way to reduce the scatter in the rainfall versus

SST relationship shown in Fig. 2 would be to restrict attention to those SSTs for which the $\theta_{e,conv}$ of the overlying atmosphere falls within a specified range (although in practice, defining $\theta_{e,conv}$ becomes more difficult as ones moves away from the inner Tropics and the mean temperature profile progressively deviates from a moist adiabat). As a step in this direction, Fig. 13 shows a scatterplot of rainfall versus SST from 1991, using data from the 10°S to 10°N latitudinal range only. The curves shown in gray are 10°S–10°N averages for an individual year between 1991 and 2000, while the dark line is for the entire period. The absence of rainfall for SSTs colder than 24°C suggests that such SSTs are incapable of generating air parcels whose θ_e exceeds the local $\theta_{e,conv}$, at least in the quantities needed to generate rain. For comparison, the dashed line in Fig. 13 shows the mean dependence of rainfall on SST from 1991 to 2000 for 30°S to 30°N.

One can use the mean dependence of convective mass on SST, together with the fractional area covered by each SST in the Tropics, to show that the average convective mass over the tropical oceans is about 76 mb. In doing this calculation, we set the convective mass at SSTs colder than 24°C equal to the value at 24°C. This estimate for convective mass is only weakly sensitive to the way this extrapolation is done because the fraction of the tropical ocean with SSTs colder than 24°C is fairly small. Between 30°S and 30°N, the fraction of the earth's surface covered by land is 24.3%. From the GPCP dataset, the fraction of the total rainfall falling over land
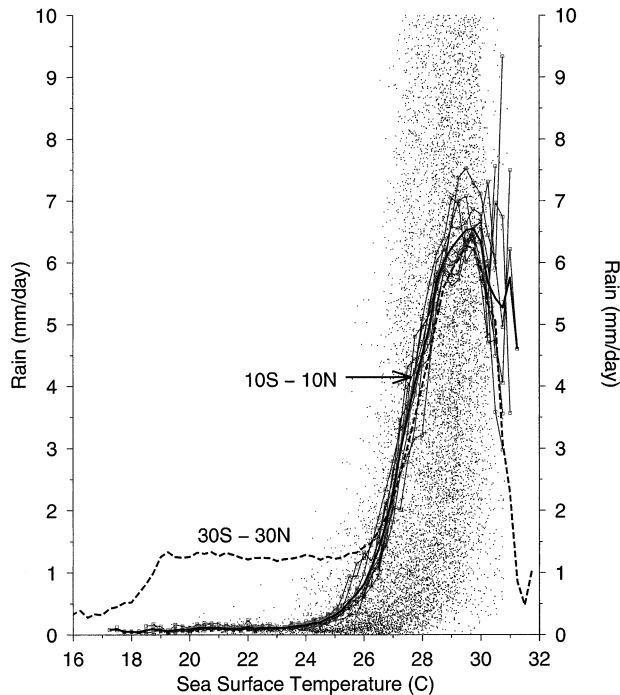
FIG. 13. A scatterplot of 1991 GPCP rainfall against Reynolds SST between 10°S–10°N. The solid black line is the mean dependence of rainfall against SST for 1991–2000, while the gray lines are averages of individual years within this time period. The dashed line is the mean 1991–2000 30°S–30°N climatology.

in this interval is 26%. Provided the convective removal timescale and the precipitation efficiency over the land and ocean are not too dissimilar, the estimate of 76 mb for the convective mass over the ocean should be close to the tropical mean. Using the previously determined estimate of 2 days for convective removal timescale suggests that the tropical mean upward mass flux in the Tropics is about 38 mb day^{-1}. This upward transport would be compensated by downward mass fluxes arising from radiative and evaporative cooling, and is consistent with a previous estimate (Betts and Ridgway 1988).

6. The statistical distribution of θ_e in the CBL

There have been a variety of attempts to look for some relationship, in actively convecting regions, between the mean surface θ_e and the potential temperature of the local tropopause. These attempts were motivated by the expectation that the air detraining from the tops of convective systems should have experienced nearly undiluted transport from the surface. There are, however, a number of reasons why one would not anticipate a clear relationship between the local mean surface θ_e and the local tropopause potential temperature. First, although one might identify a local tropopause with a local cloud-top height, the notion of a climatological tropical tropopause is problematic. The climatological profile of deep convective detrainment presumably de-

creases in some continuous manner as the tropical tropopause is approached from below. At what point does one decide that the mean detrainment rate is sufficiently weak that one is no longer in the troposphere? One criteria might be that convective detrainment is sufficiently weak that it no longer has an appreciable influence on the mean temperature profile, or the concentrations of trace gas species. One could also define the tropical tropopause as the surface, above which, the net convective outflow is small compared to the Brewer Dobson circulation. How might these surfaces be determined? It is not clear that these criteria are satisfied by conventional definitions of the tropical tropopause, either in terms of cold point or lapse rate, which were designed to identify a tropopause, from individual temperature profiles. Second, the use of a surface θ_e to determine the tropical tropopause seems arbitrary. Instead of the surface, why not use 950 mb? And finally, tropical convection can be expected to be associated with a cyclic discharging and recharging of θ_e from the CBL (Raymond 1994), with higher θ_e (positive CAPE) air parcels leaving the CBL during convection, and their replacement by lower θ_e air parcels from convective downdrafts. In this case, the use of a mean θ_e is unlikely to be representative of those air parcels from the CBL that are participating in deep convection.

It would, nevertheless, be desirable to have some way of accounting for the mean detrainment profile in the upper-tropical troposphere in terms of the thermodynamic structure of the boundary layer. If such a relationship exists, it seems most likely that the relationship is between the mean deep convective detrainment profile and some statistical measure of θ_e near the surface. In an earlier publication (Folkins 2002), clear-sky radiative heating rates were used to diagnose the detrainment profile from the diabatic divergence. It was then shown, that between 345 and 356 K (roughly 11.3–15.0 km), the rate of mass outflow between two nearby isentropic surfaces was approximately proportional to the amount of mass in the CBL between the two corresponding values of θ_e. The θ_e PDF in the CBL then becomes an important device for coupling the CBL to the upper tropical troposphere. For example, the deep convective detrainment profile can be expected to influence the mean profiles of temperature (Folkins 2002), water vapor (Folkins et al. 2002b), and ozone (Folkins et al. 2002a) in the upper tropical troposphere. On longer timescales, a relationship between the θ_e PDF of the CBL and the detrainment profile in the upper tropical troposphere may prove useful in predicting how the vertical profile of deep convective detrainment will respond to future changes in sea surface temperatures.

Figure 14 shows the response of the θ_e PDF in the CBL to SST variations in the current climate. The PDFs were obtained by grouping the radiosonde profiles from the NOAA/NCDC dataset in SST bins of 24° ± 0.5°C, ..., 30° ± 0.5°C, depending on their local monthly mean SST (Reynolds et al. 2002). There were between
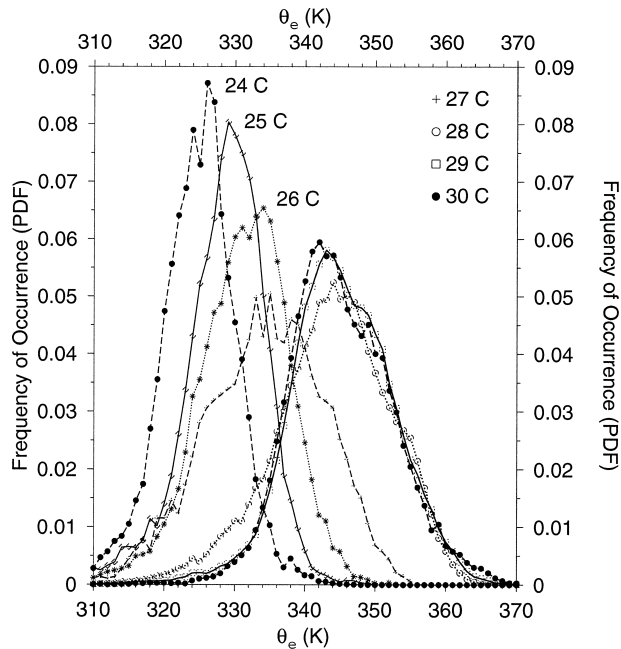
FIG. 14. PDFs of θ_e below 800 mb, averaged over various SST bins. The PDFs were calculated using radiosonde data from the locations shown in Fig. 7.

several hundred and several thousand radiosonde profiles within each SST bin. A θ_e PDF was first calculated for each 10-mb interval from 1010 to 800 mb. The PDF for that SST was then obtained by averaging over all pressure levels. This was done so that each pressure interval in the CBL contributed equally to the total PDF. Although there is a tendency for the θ_e PDFs shown in Fig. 14 to broaden and shift to higher θ_e with increasing SST, the 28°C, 29°C, and 30°C PDFs are surprisingly similar. Each is distributed roughly symmetrically about $\theta_{e,\mathrm{conv}}$, so that, on average, about half the CBL mass in actively convecting regions is able to participate in convection. The decrease in the PDFs for $\theta_e > \theta_{e,\mathrm{conv}}$, can be attributed to the convective removal of air parcels with positive CAPE from the CBL. In contrast, the peaks of those PDFs whose SST is less than 28°C tend to occur at a θ_e, which is less than the local mean $\theta_{e,\mathrm{conv}}$, so that a smaller fraction of the mass in the CBL at these cooler SSTs is able to participate in deep convection.

The fact that, in actively convecting regions, the θ_e PDF of the convecting boundary layer is symmetrically distributed about $\theta_{e,\mathrm{conv}}$ might be regarded as a consequence, or perhaps restatement, of strict quasi-equilibrium (Emanuel et al. 1994; Raymond 1994), which argues that the mean temperature profile in the Tropics is locked to the moist adiabat of the mean boundary layer θ_e in such a way as to keep the time-averaged CAPE equal to zero. Figure 14 suggests, however, that strict quasi-equilibrium only applies in actively convecting regions where the SST exceeds 28°C. Outside these re-

gions, there is no clear relationship between the mean boundary layer θ_e and $\theta_{e,\mathrm{conv}}$.

7. A Monte Carlo model of boundary layer θ_e

The convergence of the θ_e PDFs to a common form for SSTs larger than 28°C suggests that horizontal advection in these regions should not be a strong forcing on boundary layer θ_e. We therefore attempt to simulate the θ_e PDFs in these regions using a model that ignores horizontal advection and is driven purely by local forcings.

The model assumes that air parcels enter the CBL with a range of θ_e uniformly distributed between 330 and 340 K. This range was tuned to give the modeled PDFs the correct shape for $\theta_e < 340$ K. As shown in Fig. 9, it does however correspond to the range of observed θ_e at the higher SST sites at pressures between 800 and 500 mb, the pressure range over which convective downdrafts can be expected to originate. Air parcels can also enter the CBL through downward entrainment from above the CBL associated with radiative cooling. In this case, their mean θ_e would likely be closer to 340 K, but convective downdrafts are probably the dominant source of mass to the CBL in actively convecting regions. Once in the CBL, air parcels are exposed to a source of θ_e arising from the upward transport of heat and moisture from the surface, and a sink of θ_e from radiative cooling (Raymond 1995),

$$\frac{d\theta_e}{dt} = \frac{(\theta_{\mathrm{ess}} - \theta_e)}{\tau_{\mathrm{eq}}} + Q_e, \qquad (2)$$

where θ_{ess} is the saturated θ_e at the local sea surface temperature, τ_{eq} is the timescale over which the θ_e of air parcels below 800 mb becomes equilibrated with the ocean, and Q_e is radiative sink of θ_e. Here τ_{eq} can be expressed in terms of the effective wind speed U_e (Raymond 1995)

$$\tau_{\mathrm{eq}} = \frac{b}{C_d U_e}, \qquad (3)$$

where b is the depth of the CBL (~ 2000 m), and $C_d \approx 10^{-3}$ is the drag coefficient. We set $Q_e = -2$ K day^{-1} (e.g., Betts and Ridgway 1988; Raymond 1994).

Once the θ_e of an air parcel becomes larger than $\theta_{e,\mathrm{conv}}$, air parcels are subject to removal from the CBL with a probability equal to dt/τ_{rem}, where dt is the model time step and τ_{rem} is a convective removal timescale. As discussed earlier, the ratio of convective water to rainfall in actively convecting regions suggests $\tau_{\mathrm{rem}} \sim 2$ days, provided one assumes a precipitation efficiency of 60%. The model generates a θ_e PDF by injecting several thousand air parcels into the CBL, with an input range of θ_e, as mentioned earlier, between 330 and 340 K. The air parcels are subjected to the θ_e forcings given in (2), and a PDF constructed by keeping track of how much time the air parcels spend at each value of θ_e. The model

TABLE 1. The parameters of the Monte Carlo model. Note that some of the parameters are not independent. Here θ_{ess} is derived from the mean SST (Bolton 1980); $\theta_{e,max}$ is derived from θ_{ess}, Q_e, and τ_{eq} using a formula from the text; and τ_{eq} is derived from the observed effective mean surface wind speed U_e.

Parameter	SST value		
	28° ± 0.5°C	29° ± 0.5°C	30° ± 0.5°C
Mean SST	28.2°C	29.1°C	29.7°C
θ_{ess}	369.8 K	375.0 K	378.3 K
$\theta_{e,conv}$	342.0 K	343.8 K	344.4 K
$\theta_{e,max}$	362.8 K	365.9 K	367.1 K
U_e ($ws < 100$ m)	6.7 m s^{-1}	5.1 m s^{-1}	4.1 m s^{-1}
τ_{eq}	3.5 days	4.5 days	5.6 days
τ_{rem}	2.0 days	2.0 days	2.0 days
Q_e	−2 K day^{-1}	−2 K day^{-1}	−2 K day^{-1}
Range of input θ_e	330–340 K	330–340 K	330–340 K

is mass conserving by construction, since it sequentially injects and removes individual air parcels. The rates at which the model removes mass and water vapor from the CBL by convection should be realistic if the θ_e PDFs generated by the model are similar to those observed. There is no explicit mixing between individual air parcels in the model, though mixing is presumably one of mechanisms by which the θ_e of each air parcel is equilibrated with the θ_{ess} of the underlying ocean. The time step was chosen to be 0.02 days.

The model has seven parameters: θ_{ess}, $\theta_{e,conv}$, θ_e, τ_{eq}, Q_e, τ_{rem}, and the upper and lower limit input injection θ_e values. One model run was made for each of the 28 ± 0.5°C, 29 ± 0.5°C, and 30 ± 0.5°C bins. During each model run, Q_e, τ_{rem}, and the upper and lower limit θ_e values were kept fixed at the values given above, $\theta_{e,conv}$ and τ_{eq} were constrained by radiosonde measurements, and θ_{ess} was calculated from the average SST within the SST bin. The equilibrium timescale τ_{eq} was calculated from (3), with the effective wind speed U_e obtained from the radiosonde measurements by averaging over all wind speed measurements below 100 m within the SST bin. Table 1 shows the values of the seven model parameters for each SST run.

Figure 15 shows some of the θ_e "trajectories" generated by the model for the 28°C SST run. Trajectories start to be removed once their θ_e exceeds $\theta_{e,conv}$. Note that the rate of increase of θ_e is progressively reduced at large θ_e, so that θ_e approaches a limiting value θ_{max}, which from (2) can be shown to equal

$$\theta_{e,max} = \theta_{ess} + Q_e\tau_{eq}. \tag{4}$$

As shown in Table 1, the maximum possible θ_e in the CBL is reduced, in the case of an SST of 28°C, by 7 K from the amount one would anticipate based on the local sea surface temperature. This reduction may account for some of the difficulties encountered in attempting to estimate maximum cloud-top potential temperatures based on SST alone (e.g., Reid and Gage 1981; Chimonas and Rossi 1987). Such estimates do not take
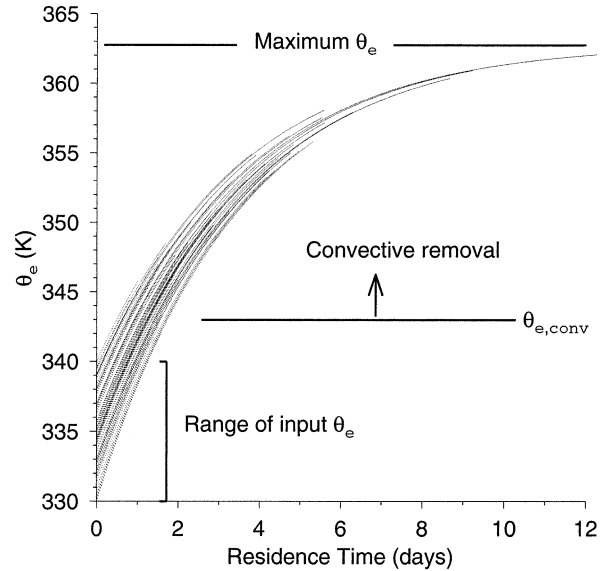

FIG. 15. Several θ_e trajectories from the Monte Carlo model. Air parcels are injected into the boundary layer with initial θ_e between 330 and 340 K. Their θ_e is increased by heat and moisture fluxes from the surface and decreased by radiative cooling. Air parcels are subject to convective removal from the boundary layer once their θ_e exceeds the local $\theta_{e,conv}$. The expression for the maximum possible θ_e is given in the text.

into consideration the fact that air parcels can only spend a finite amount of time in the boundary layer, and are continuously subjected to a sink of θ_e from radiative cooling.

Using Eqs. (3) and (4), and assuming $U_e = 5$ m s^{-1} and $Q_e = -2$ K day^{-1} it can be shown that $\theta_{e,max} = 340$ K for an SST of 24°C. Figure 12 shows that the smallest possible value of $\theta_{e,conv}$ in the inner Tropics is 340 K, suggesting that SSTs colder than 24°C in the inner Tropics are thermodynamically incapable of supporting convection. This is consistent, as shown in Fig. 13, with the absence of rainfall at these SSTs.

Figure 16 shows the monthly mean wind speed plotted against SST for each of the 12 radiosonde locations. Wind speeds decrease by almost a factor of two in going from an SST of 28° to 30°C. One would expect low wind speeds to be associated with high SSTs, both because high SST regions tend to be located near the center of large-scale low-level convergence patterns, and because the suppression of latent heat fluxes at low wind speeds would give rise to positive SST anomalies (Zhang and McPhaden 1995; Zhang et al. 1995). Simplified models of the tropical boundary layer, coupled to an interactive ocean, have been used to predict a relationship between SST and wind speed, which for high SSTs, is similar to that shown in Fig. 16 (Betts and Ridgway 1989). Table 1 shows the increase in τ_{equil} at high SST associated with the reduction in wind speed.

Figure 17 shows the observed θ_e PDFs for each of the three SST bins, and the PDFs generated by the model (solid circles). At low θ_e, the agreement between the
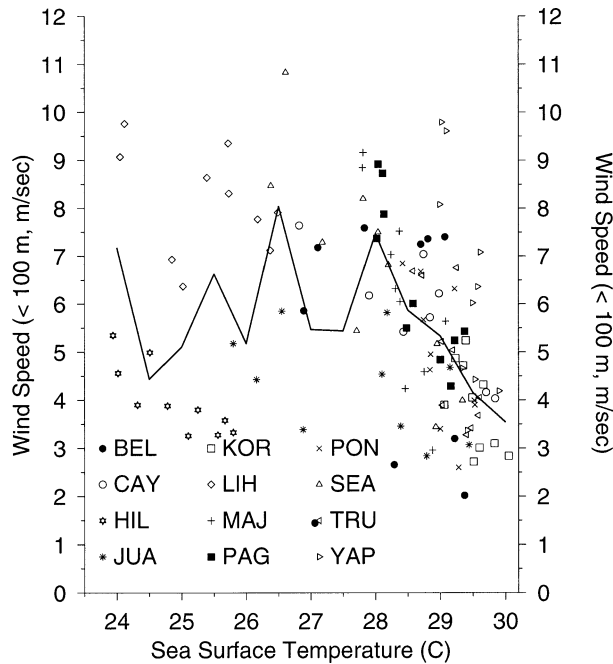
FIG. 16. Monthly mean wind speed (below 100 m) against monthly mean SST at various radiosonde locations. The solid line corresponds to the average wind speed in 0.5°C intervals. The locations corresponding to the three letter codes are shown in Fig. 7.
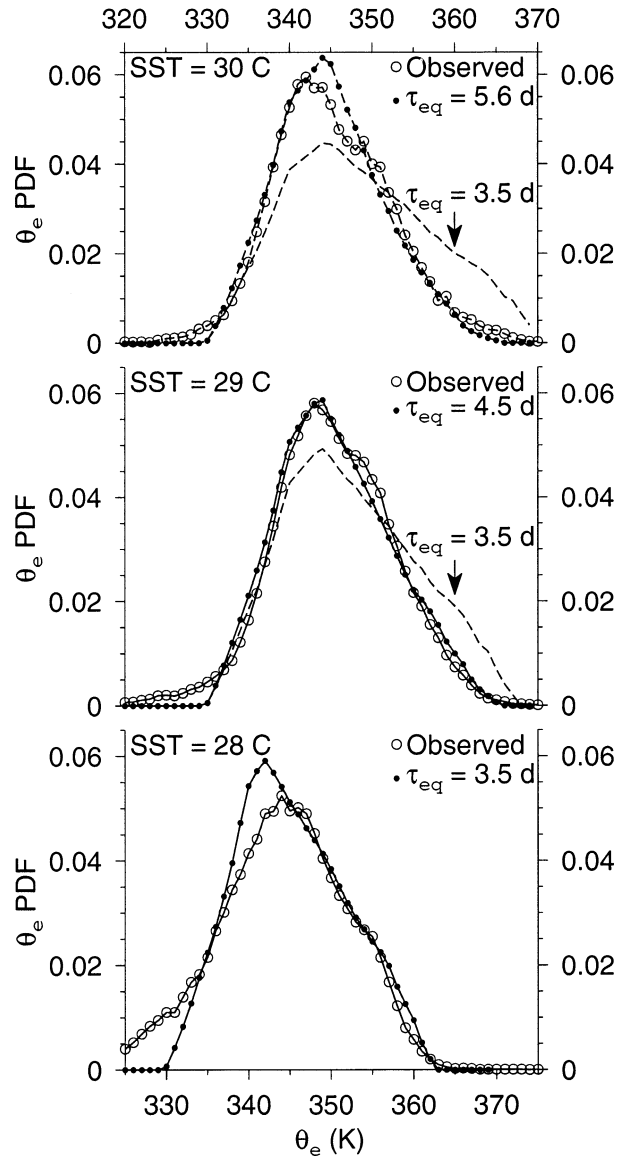

FIG. 17. In each plot, the curve with open circles corresponds to the observed θ_e PDF at that SST (also shown in Fig. 14). The lines with solid circles show the θ_e PDFs generated by the Monte Carlo model, with the parameters of the model constrained by radiosonde measurements in that SST bin. The dashed lines of the middle and upper panel denote the PDFs generated by the model with τ_{equil} fixed at 3.5 days. They are intended to represent what the θ_e PDFs would look like if the surface wind speed were constant above 28°C.

modeled and observed PDFs is a consequence of the particular choice of input θ_e values (330 to 340 K). At large θ_e, however, the shape of the modeled PDFs is mainly determined by the values of θ_{ess}, the convective threshold θ_e, τ_{eq}, Q_e, and τ_{rem}. Each of these five parameters is constrained by independent measurements, or in the case of the radiative heating rate Q_e, a commonly accepted model result.

The dashed curves in the middle (29° ± 0.5°C) and upper (30° ± 0.5°C) panels of Fig. 17 show the θ_e PDFs generated by the model when the equilibrium timescale τ_{eq} for these SST bins is set equal to 3.5 days, the value of τ_{eq} used in the 28° ± 0.5°C SST run. In these two cases, the model generates a much less symmetric distribution in which the frequency of high θ_e air parcels is much higher than observed. This suggests that the tendency, in actively convecting regions, for wind speeds to decrease with increasing SST partially accounts for the convergence of the θ_e PDFs in these regions to a common shape that is independent of SST. This shape invariance is, of course, also due to the tendency for temperatures in the inner Tropics to be horizontally homogeneous. This clamps the peaks of the PDFs to a common value equal to the local $\theta_{e,conv}$. The homogeneity of inner tropical temperatures also helps ensure that the range of input θ_e entering the boundary layer from convective downdrafts does not depend on SST.

The success of the model in reproducing the observed θ_e PDFs in actively convecting regions supports the no-

tion that, over the western Pacific warm pool, one reaches a regime in which there is a local balance between the injection of low θ_e air into the CBL (mainly from convective downdrafts), a source from the surface, radiative cooling, and the removal of parcels whose θ_e exceeds $\theta_{e,conv}$ by deep convection (Raymond 1995). The model also gives some insight into the existence of a fixed point in actively convective regions, in which the θ_e PDF of the boundary layer becomes unresponsive to changes in the underlying SST. Provided one constrains

the Monte Carlo model by the observed wind speeds, the frequency of occurrence of very high θ_e air parcels is also very close to that observed.

However, when applied to SSTs lower than 28°C, the model fails to reproduce the shapes of the observed θ_e PDFs and overpredicts the convective mass. The most likely reason for these failures is that the model assumes an air parcel will remain in the convective boundary layer until its θ_e exceeds the local $\theta_{e,\text{conv}}$, at which time it becomes subject to convective removal. For SSTs lower than 28°C, however, the peak of the θ_e PDF is lower than $\theta_{e,\text{conv}}$, indicating that convection is probably not the dominant mechanism by which air is removed from the boundary layer in these regions. Presumably, the timescale required for an an air parcel to exceed the local $\theta_{e,\text{conv}}$ is comparable with the timescale required for an air parcel in the CBL to be advected to a region of higher SST, so that a purely local balance is never realized.

8. Discussion

There appears to be a natural partitioning of the tropical oceans into weakly and actively convecting regimes. In the weakly convecting regime, convection is infrequent, and associated with dynamical fluctuations that lower the local $\theta_{e,\text{conv}}$. In the actively convecting regime, convection is quasi-continuous and the PDF of θ_e in the boundary layer assumes a shape that is independent of SST. The peak of this PDF is directly coupled to the mean temperature profile of the inner Tropics.

The transition between the weakly and actively convecting regimes occurs near 26°C and is quite sharp. We have argued that this can be understood as a response to an increase in the amount of mass in the CBL whose θ_e exceeds $\theta_{e,\text{conv}}$.

In an idealized tropical atmosphere, where atmospheric temperatures were perfectly homogeneous and boundary layer θ_e could be characterized by a single value, there would be a discontinuous increase in rainfall at the convective threshold SST. Factors that smooth out the transition include the tendency for convection to give rise to a local increase in the temperature of the atmosphere, dynamically induced fluctuations in mid-tropospheric temperatures, and anything that contributes toward broadening the PDF of boundary layer θ_e.

In the weakly convecting regime, surface winds will be generally directed from colder to warmer SSTs. Horizontal advection will therefore give rise to a net negative tendency on boundary layer θ_e. It seems likely that this negative tendency plays a significant role in suppressing convection in the weakly convecting regime. Within the actively convecting regime, the PDF of boundary layer θ_e is independent of SST, so that horizontal advection does not play a role in the mean θ_e budget. An increase in the horizontal advection tendency from negative to near-zero values in the vicinity of the SST threshold probably sharpens the transition from

the weakly to actively convecting regimes. Certainly, it is difficult to understand, from the perspective of a purely local water vapor budget, how the nonlinear dependence of tropical rainfall on sea surface temperatures might be reconciled with the absence of a corresponding feature in the latent heat flux. Moreover, simplified models of the Tropics have recently emphasized the importance of horizontal advection of boundary layer moisture in determining the value of the convective threshold SST (Sobel and Bretherton 2000; Bretherton and Sobel 2002). Turning off horizontal moisture advection in these models decreases the convective threshold SST to a lower value, and makes the onset of precipitation at the threshold SST much more gradual.

We have attibuted, at least in part, the common shape of the mean boundary layer θ_e PDFs in actively convecting regions to the suppression of low-level wind speeds at higher SSTs. But we have not attempted to determine the origin of this relationship. If, however, low-level wind speeds did not decrease at high SSTs, these regions would have a much higher prevalence of very high θ_e (> 360 K) air parcels. And, unless the convective removal timescales in these regions were for some reason longer than elsewhere, this would be associated with enhanced fluxes of latent and sensible heat from the ocean surface. The existence of a common shape for the mean θ_e PDFs in actively convecting regions may therefore arise from considerations associated with maintaining local energy balance.

The two main weaknesses of this analysis are the existence of unresolved biases in relative humidity measurements of the tropical CBL, and the poor geographical representativeness of the radiosonde stations. This is due to the lack of radiosonde stations on tropical islands reporting at high resolution in the tropical Atlantic and Indian Oceans. It would be especially helpful to have a greater number of radiosonde measurements from sites in the vicinity of the SST threshold, or field campaigns that examined the moist entropy budget of the tropical boundary layer near the transition. Understanding the transition from the weakly to actively convecting regimes is important, in part, because midlatitude weather patterns can be expected to be especially sensitive to movements in the position of the convective threshold SST contour, and because the value of the SST threshold is not always accurately simulated by current coupled ocean–atmosphere models (e.g., Dutton et al. 2000).

REFERENCES

Betts, A. K., and W. Ridgway, 1988: Coupling of the radiative, convective, and surface fluxes over the equatorial Pacific. *J. Atmos. Sci.,* **45,** 522–536.

——, and ——, 1989: Climatic equilibrium of the atmospheric convective boundary layer over a tropical ocean. *J. Atmos. Sci.,* **46,** 2621–2641.

Bjerknes, J., 1966: A possible response of the atmospheric Hadley circulation to equatorial anomalies of ocean temperature. *Tellus,* **18,** 820–829.

Bolton, D., 1980: The computation of equivalent potential temperature. *Mon. Wea. Rev.,* **108,** 1046–1053.

Bretherton, C. S., and A. H. Sobel, 2002: A simple model of a convectively coupled Walker circulation using the weak temperature gradient approximation. *J. Climate,* **15,** 2907–2920.

Chimonas, G., and R. Rossi, 1987: The relationship between tropopause potential temperature and the buoyant energy of storm air. *J. Atmos. Sci.,* **44,** 2902–2911.

Dutton, J. F., C. J. Poulsen, and J. L. Evans, 2000: The effect of global climate change on the regions of tropical convection in CSM1. *Geophys. Res. Lett.,* **27,** 3049–3052.

Emanuel, K. A., 1994: *Atmospheric Convection.* Oxford University Press, 580 pp.

——, J. D. Neelin, and C. S. Bretherton, 1994: On large-scale circulations in convecting atmospheres. *Quart. J. Roy. Meteor. Soc.,* **120,** 1111–1143.

Folkins, I., 2002: Origin of lapse rate changes in the upper tropical troposphere. *J. Atmos. Sci.,* **59,** 992–1005.

——, C. Braun, A. M. Thompson, and J. White. 2002a: Tropical ozone as an indicator of deep convection. *J. Geophys. Res.,* **107** (D13), 4184, doi:10.1029/2001JD001178.

——, K. K. Kelly, and E. M. Weinstock, 2002b: A simple explanation for the increase in relative humidity between 11 and 14 km in the Tropics. *J. Geophys. Res.,* **107** (D23), 4736, doi:10.1029/2002JD002185.

Gadgil, S., P. V. Joseph, and N. V. Joshi, 1984: Ocean–atmosphere coupling over monsoon regions. *Nature,* **312,** 141–143.

Gill, A. E., and E. M. Rasmusson, 1983: The 1982–83 climate anomaly in the equatorial Pacific. *Nature,* **306,** 229–234.

Graham, N. E., and T. P. Barnett, 1987: Sea surface temperature, surface wind divergence, and convection over tropical oceans. *Nature,* **238,** 657–659.

Huffman, G. J., and Coauthors, 1997: The Global Precipitation Climatology Project (GPCP) Combined Precipitation Data Set. *Bull. Amer. Meteor. Soc.,* **78,** 5–20.

Ichiye, T., and J. R. Petersen, 1963: The anomalous rainfall of the

1957–58 winter in the equatorial central Pacific arid area. *J. Meteor. Soc. Japan, Ser. II,* **41,** 172–182.

Kiladis, G. N., and K. M. Weickmann, 1992: Circulation anomalies associated with tropical convection during northern winter. *Mon. Wea. Rev.,* **120,** 1900–1923.

Neelin, J. D., and I. M. Held, 1987: Modeling tropical convergence based on the moist static energy budget. *Mon. Wea. Rev.,* **115,** 3–12.

Newell, R. E., 1979: Climate and the ocean. *Amer. Sci.,* **67,** 405–416.

Ramage, C. S., 1977: Sea surface temperature and local weather. *Mon. Wea. Rev.,* **105,** 540–544.

Ramanathan, V., and W. Collins, 1991: Thermodynamic regulation of ocean warming by cirrus clouds deduced from observations of the 1987 El Niño. *Nature,* **351,** 27–32.

Raymond, D., 1994: Convective processes and tropical atmospheric circulations. *Quart. J. Roy. Meteor. Soc.,* **120,** 1431–1455.

——, 1995: Regulation of moist convection over the west Pacific warm pool. *J. Atmos. Sci.,* **52,** 3945–3959.

——, 2000: Thermodynamic control of tropical rainfall. *Quart. J. Roy. Meteor. Soc.,* **126,** 889–898.

Reid, G. C., and K. S. Gage, 1981: On the annual variation in height of the tropical tropopause. *J. Atmos. Sci.,* **38,** 1928–1938.

Reynolds, R. W., N. A. Rayner, T. M. Smith, D. C. Stokes, and W. Wang, 2002: An improved in situ and satellite SST analysis for climate. *J. Climate,* **15,** 1609–1625.

Slingo, J. M., 1998: Extratropical forcing of tropical convection in a northern winter simulation with the UGAMP GCM. *Quart. J. Roy. Meteor. Soc.,* **124,** 27–51.

Sobel, A. H., and C. S. Bretherton, 2000: Modeling tropical precipitation in a single column. *J. Climate,* **13,** 4378–4392.

Waliser, D. E., 1996: Formation and limiting mechanisms for very high sea surface temperature: Linking the dynamics and the thermodynamics. *J. Climate,* **9,** 161–188.

——, N. E. Graham, and C. Gautier, 1993: Convective cloud systems and warm-pool sea surface temperatures: Coupled interactions and self-regulation. *J. Geophys. Res.,* **98,** 12 881–12 893.

Wang, J., H. L. Cole, D. J. Carlson, E. Miller, K. Beierle, A. Paukkurien, and T. K. Laine, 2002: Corrections of humidity measurement errors from the Vaisala RS80 radiosonde—Application to TOGA COARE data. *J. Atmos. Oceanic Technol.,* **19,** 981–1002.

Weare, B. C., 1987: Relationships between monthly precipitation and SST variations in the tropical Pacific region. *Mon. Wea. Rev.,* **115,** 2687–2698.

Xu, K., and K. A. Emanuel, 1989: Is the tropical atmosphere conditionally unstable? *Mon. Wea. Rev.,* **117,** 1471–1479.

Zhang, C., 1993: Large-scale variability of atmospheric deep convection in relation to sea surface temperature in the Tropics. *J. Climate,* **6,** 1898–1913.

Zhang, G. J., and M. J. McPhaden, 1995: The relationship between sea surface temperature and latent heat flux in the equatorial Pacific. *J. Climate,* **8,** 589–605.

——, V. Ramanathan, and M. J. McPhaden, 1995: Convection–evaporation feedback in the equatorial Pacific. *J. Climate,* **8,** 3040–3051.